Molecular Cancer Therapeutics

Blood Interactions, Pharmacokinetics, and Depth-Dependent Ablation of Rat Mammary Tumors with Photoactivatable, Liposomal Doxorubicin

Kevin A. Carter[1], Dandan Luo[1], Jumin Geng[1], Stephan T. Stern[2], and Jonathan F. Lovell[1]

Abstract

Photosensitizers can be integrated with drug delivery vehicles to develop chemophototherapy agents with antitumor synergy between chemo- and photocomponents. Long-circulating doxorubicin (Dox) in porphyrin–phospholipid (PoP) liposomes (LC-Dox-PoP) incorporates a phospholipid-like photosensitizer (2 mole %) in the bilayer of Dox-loaded stealth liposomes. Hematological effects of endotoxin-minimized LC-Dox-PoP were characterized via standardized assays. *In vitro* interaction with erythrocytes, platelets, and plasma coagulation cascade were generally unremarkable, whereas complement activation was found to be similar to that of commercial Doxil. Blood partitioning suggested that both the Dox and PoP components of LC-Dox-PoP were stably entrapped or incorporated in liposomes. This was further confirmed with pharmacokinetic studies in Fischer rats, which showed the PoP and Dox components of the liposomes both had nearly identical, long circulation half-lives (25–26 hours). In a large orthotopic mammary tumor model in Fischer rats, following intravenous dosing (2 mg/kg Dox), the depth of enhanced Dox delivery in response to 665 nm laser irradiation was over 1 cm. LC-Dox-PoP with laser treatment cured or potently suppressed tumor growth, with greater efficacy observed in tumors 0.8 to 1.2 cm, compared with larger ones. The skin at the treatment site healed within approximately 30 days. Taken together, these data provide insight into nanocharacterization and photo-ablation parameters for a chemophototherapy agent.

Introduction

The delivery of anticancer agents at therapeutically relevant concentrations is a major challenge in treating solid tumors (1–4). Nanoparticles, particularly liposomes, have been widely used clinically to address this concern (5–8). However, nanoparticles do not necessarily provide enhanced therapeutic effects over the free drug; rather, they provide a reduction in toxicity and alteration of pharmacokinetics (9–13). Doxil, a PEGylated liposomal form of doxorubicin (Dox), for example, is clinically approved for the treatment of Kaposi sarcoma, ovarian cancer, and multiple melanoma (14), and is widely used for the treatment of metastatic breast cancer (15). Yet it does not offer clearly superior efficacy over non-liposomal doxorubicin (9, 16–19). Rather, its use is driven by a reduction in side-effects compared with free Dox, including cardiotoxicity (9, 17). This lack of greater efficacy, despite enhanced delivery to the tumor, is attributed to poor bioavailability of liposome-encapsulated drugs due to their slow release (9, 20). Numerous molecular-targeting strategies have been explored for liposomes (21–24). Alternatively, several stimulus controlled systems have been developed to address this problem, including systems that use heat, light, and pH to trigger drug release (25–31). The most advanced of which, Thermodox, a heat-triggered, liposome-encapsulated Dox, has been tested clinically for the treatment multiple forms of cancer, including liver cancer and breast cancer (32–34). The combination of light therapy and chemotherapy, chemophototherapy (CPT), is an emerging treatment paradigm for solid tumors (35). Photodynamic therapy (PDT) itself is a clinically used ablative modality that has been shown to treat a variety of tumor types (36, 37).

We previously described long-circulating Dox in porphyrin–phospholipid (LC-Dox-PoP) liposomes, a PEGylated liposomal form of Dox, co-encapsulated with a bilayer-confined and lipid-like porphyrin–phospholipid (PoP) conjugate incorporated at 2 mole % (total lipid). In murine studies, LC-Dox-PoP liposomes were shown to have long circulating properties similar to that of sterically stabilized stealth liposomal doxorubicin, and enhanced antitumor efficacy when combined with laser treatment, at doses significantly lower than Doxil-like liposomes (38–40). Here, we report *in vitro/in vivo* biological evaluation of the LC-Dox-PoP liposomes, including *in vitro* immunological characterization, blood partitioning, *in vivo* pharmacokinetics, and antitumor efficacy in an orthotopic rat tumor model with specific emphasis on determining the suitability of LC-Dox-PoP for use in humans.

Materials and Methods

Liposome preparation

LC-Dox-PoP liposomes were prepared as previously described (38). Briefly, 200 mg of lipids were dissolved in 2 mL

[1]Department of Biomedical Engineering, University at Buffalo, State University of New York, Buffalo, New York. [2]Nanotechnology Characterization Laboratory, Cancer Research Technology Program, Frederick National Laboratory for Cancer Research sponsored by the National Cancer Institute, Frederick, Maryland.

Note: Supplementary data for this article are available at Molecular Cancer Therapeutics Online (http://mct.aacrjournals.org/).

Corresponding Author: Jonathan F. Lovell, 210 Bonner Hall, University at Buffalo, State University of New York, Buffalo, NY, 14260. Phone: 716-645-1020; E-mail: jflovell@buffalo.edu

doi: 10.1158/1535-7163.MCT-18-0549

of ethanol in the molar ratio [53:2:5:40; 1,2-distearoyl-sn-glycero-3-phosphocholine (**DSPC**, Corden LP-R4-076):**pyro-lipid** (synthesized as previously described; ref. 38)]: 1,2-distearoyl-sn-glycero-3-phosphoethanolamine-N-[methoxy(polyethylene glycol)-2000] (**DSPE-PEG-2000**, Corden, LP-R4-039): cholesterol (**Chol**, PhytoChol; Wilshire Technologies, CAS 57-88-5)]. The solution of dissolved lipids was heated to 60°C and 8 mL of 250 mmol/L ammonium sulfate (60°C) was added to the ethanol. The liposomes were then extruded 10 times using a 10 mL nitrogen pressurized extruder (Northern Lipids) using stacked (80, 100, and 200 nm) polycarbonate membranes at 60°C. Excess ammonium sulfate and ethanol were removed by dialysis (MWCO 12,000-14,000, Fisher # 21-152-16) in a buffer of 10 mmol/L histidine (pH 6.5), 10% sucrose solution with three buffer changes. Dox (LC Laboratories # D-4000) was encapsulated into the liposomes by mixing the liposome and Dox solution, and incubating for 60 minutes at 60°C. Following Dox loading, liposomes were sterile filtered using a 0.2-μm Supor membrane filter (Pall # 28143-300). Doxil was obtained from the NIH pharmacy.

Liposome characterization

Liposome size and zeta potential. A Malvern Zetasizer Nano ZS instrument (Southborough, MA) was used for measuring the hydrodynamic size (diameter) and zeta potential in accordance to National Institute of Standards and Technology (NIST)—National Cancer Institute Nanocharacterization laboratory (NCL) joint protocol PCC-1 and NCL protocol PCC-2, respectively. Hydrodynamic size was measured by diluting the liposomes 100- and 1,000-fold in PBS or 10 mmol/L NaCl (zeta potential measurement conditions). Samples were measured at 25°C in a quartz microcuvette with a back scattering detector (173°) in batch mode. Zeta potential was measured by diluting the liposomes 100-fold in 10 mmol/L NaCl. Sample pH was measured before loading into a pre-rinsed folded capillary cell. Measurements were made at both native pH and after adjustment to neutral pH using 1 N standardized NaOH. An applied voltage of 150 V was used.

Liposome morphology. Cryo-transmission electron microscopy (cryo-TEM) was performed to assess the morphology of the liposomes. To prepare the sample for cryo-TEM, 4 μL of stock solution or solution diluted ×20 in ultrapure water was applied to a quantifoil holey film 200 mesh copper grid (Electron Microscopy Sciences) and blotted either for 3 or 2.5 sec, respectively, before plunge freezing in liquid ethane using a Vitrobot (FEI Company) to form a thin film of vitreous ice. Imaging was performed using a Tecnai T-20 equipped with a tungsten thermoionic gun using low-dose mode.

Doxorubicin encapsulation efficiency. Encapsulation efficiency of doxorubicin was assessed using UV-Vis spectroscopy and centrifugal filtration to measure free doxorubicin. Samples (250 μL) were centrifuged at 14,000 rpm at 24°C to dryness using Microcon DNA Fast Flow centrifugal devices (Millipore, MRCFOR100, RC). The filtrate, containing any free doxorubicin, was analyzed by UV-Vis spectroscopy. UV-Vis spectra were recorded using a PerkinElmer Lambda 35 spectrophotometer. All samples were measured in quartz microcuvettes (path length, $b = 10$ mm, QS105.250). Spectra were collected from 200 to 800 nm at 480 nm/min in 1-nm steps against water as the reference. Calibration standards of doxorubicin were prepared from a 2,000 μg/mL doxorubicin stock solution in 25 mmol/L NaCl. Calibration standards were prepared by diluting this calibration stock with 25 mmol/L NaCl to final concentrations ranging from 5 to 50 μg/mL. Doxorubicin calibration standards were subjected to the same centrifugation process as the liposome samples.

Hemolysis

Hemolysis tests were conducted *in vitro* in accordance to the NCL protocol "ITA-1, Analysis of Hemolytic Properties of Nanoparticles." In brief, freshly drawn human blood anticoagulated with lithium heparin was diluted in PBS to a concentration of 10 mg/mL total blood hemoglobin. The diluted whole blood was then incubated with test samples for 3 hours at 37°C. Following incubation, cell-free supernatants were prepared and analyzed for the presence of plasma-free hemoglobin by converting hemoglobin and its metabolites into cyanmethemoglobin (CMH) using Drabkin's reagent. CMH was then quantified against a hemoglobin standard by measuring the absorbance of the samples at 540 nm.

Platelet aggregation

Platelet aggregation tests were conducted *in vitro* in accordance to NCL protocol "ITA-2, Analysis of Platelet Aggregation." In brief, platelet-rich plasma (PRP) and platelet-poor plasma (PPP) were prepared from freshly drawn human blood. PPP was used as the background control. PRP was incubated with the ChronoLum reagent and test samples, and sample turbidity was measured using the ChronoLog aggregometer. The ChronoLum reagent was used to monitor ATP release from platelets. The latter correlates with platelet aggregation and is used as an additional control to verify that any changes observed in the light transmission were due to platelet aggregation.

Plasma coagulation

Plasma coagulation tests were conducted *in vitro* in accordance with NCL protocol "ITA-12, Coagulation Assay." In brief, three plasma coagulation tests were performed, prothrombin time (PT), activated partial thromboplastin time (APTT), and thrombin time (TT). Freshly drawn human blood was used to prepare plasma. Control N (normal plasma standard) and control P (abnormal plasma standard) were obtained as citrated human plasma from a commercial source specializing in the clinical diagnostic blood coagulation products (Diagnostica Stago). The controls are verified by the manufacturer against relevant standards so that coagulation time of the Control N is below and that of the Control P is above the threshold normal coagulation time for the given plasma coagulation assay. Plasma was incubated with test samples for 30 minutes at 37°C. Following incubation, plasma coagulation initiation reagents (neoplastin, $CaCl_2$, or thrombin, respectively) were added to the mixture and the coagulation times measured using the STArt4 coagulometer (Diagnostica Stago).

Complement activation

Complement activation tests were conducted *in vitro* in accordance with NCL protocol "ITA-5.2, Analysis of Complement Activation by EIA." Briefly, plasma was prepared from freshly drawn human blood and incubated with test samples and veronal buffer for 30 minutes at 37°C. Following incubation, the samples were analyzed for the presence of the iC3b component of complement using a commercial enzyme immunoassay kit.

LC-Dox-PoP liposomes were analyzed at four concentrations ranging 0.002 to 0.66 mg/mL Dox. Doxil was used as an additional, commercially relevant nanoparticle control. Doxil was tested at equivalent Dox concentrations.

Blood partitioning

A previously described blood partitioning method (41) was used to determine the percentage of plasma fraction for both PoP and Dox, using the equation $F_P\% = (C_P/C_B)(1\text{-HCT}) \times 100$, where C_P = concentration in plasma; C_B = concentration in the blood; and HCT = hematocrit. Fresh human blood was collected in K2-EDTA tubes (Thermo Fischer Scientific, Waltham, MA, Cat. # 02-689-4) for these studies. For analysis in whole blood, 3 mL blood was spiked with LC-Dox-PoP liposomes, in triplicate, to yield final concentrations of 0.5, 2, and 10 μg PoP/mL, corresponding to 2.5, 10.2, and 51.2 μg Dox/mL, in glass vials. Samples were incubated at 37°C with agitation. At specified time points (time zero, 30 minutes, 2, 4, and 24 hours), 50 μL blood was taken for PoP and Dox analysis. A capillary sample was also taken for hematocrit measurement. For plasma analysis, 500 μL of blood was also taken at each time point above, transferred to an Eppendorf tube and spun at 2,500 x *g* for 10 minutes to collect plasma. Plasma (50 μL each) was sampled for PoP and Dox analysis using LC-MS. See Supplementary Information for detailed LC-MS methods.

Pharmacokinetic studies

Before injection, LC-Dox-PoP liposomes were diluted in PBS to a concentration of 1 mg Dox/mL. Double jugular catheterized 10-week-old male Fischer 344 rats (approximately weight of 250 grams) were purchased from Charles River Laboratories. Six rats were treated intravenously by left catheter with 5 mg Dox/ 2.4 mg PoP/5 mL/kg LC-Dox-PoP liposomes. Blood samples (250 μL) were collected in K2EDTA tubes by the right jugular catheter at 0.25, 0.5, 1, 2, 4, 8, 24, and 48 hours after injection, and spun to collect plasma and stored at −80°C. Plasma from the untreated control animals was also collected and used to prepare plasma matrix standard curve, and quality control standards. Frozen plasma samples were prepared for PoP and Dox analysis by LC-MS. See Supplementary Information for detailed LC-MS methods.

Pharmacokinetic analysis

Noncompartmental pharmacokinetic parameters were determined using Phoenix WinNonlin Version 6.3 software (Pharsight Corporation): The area under the time concentration curve (AUC_{inf}) was calculated using the linear trapezoidal rule with extrapolation to time infinity; total clearance (CL) was calculated from dose/AUC_{inf}; terminal half-life ($t_{1/2}$) was calculated from 0.693/slope of the terminal elimination phase; the C_{max} term is the maximum concentration; volume of distribution steady-state (V_{ss}) was calculated from (dose/AUC_{inf}) × [area under the first moment curve (AUMC)/AUC_{inf}]; mean residence time (MRT) was calculated as (AUMC)/AUC_{inf}).

Biodistribution and tumor drug deposition

Female Fischer 344 rats were inoculated with orthotopic R3230 mammary adenocarcinoma tumors on both the left and right sides skin immediately adjacent to the base of the most caudal pair of nipples. R3230 cells were provided as a kind gift from Dr. Nahum Goldberg (Beth Israel Deaconess Medical Center) and were maintained for tumor studies without authentication. Once the tumors were approximately 20 mm (2 cm) in diameter, rats were injected intravenously with 2 mg/kg LC-Dox-PoP liposomes and 1 hour after injection, tumors irradiated with a 665 nm laser diode (RPMC laser, LDX-3115-665) at a fluence rate of 150 mW/cm^2 (total fluence: 250 J/cm^2). Twenty-four hours after laser treatment rats were sacrificed, and tumors and key organs surgically excised. PoP and Dox tissue concentrations were analyzed using previously described fluorescence methods (38). To measure the drug concentration as a function of tumor depth tumors were sliced into 2-mm segments starting from the side adjacent to skin.

Tumor growth inhibition

Female Fischer 344 rats were inoculated with 5×10^6 R3230 mammary adenocarcinoma cells in a volume of 100 μL injected through the skin immediately adjacent to the base of the most caudal pair of nipples. Once the tumors were large enough (8–12 mm or 12–16 mm depending on the treatment group) the rats were injected intravenously with 2 mg/kg LC-Dox-PoP liposomes, or an equivalent dose of empty PoP liposomes, and tumors irradiated with a 665 nm laser diode (RPMC laser, LDX-3115-665) at a fluence rate of 150 mW/cm^2 (250 J/cm^2) 1 hour after injection. Tumor size was monitored 2 to 3 times per week and tumor volumes calculated using caliper measurements and the formula: $V = \pi/6 \cdot L \cdot W^2$, where V, L, and W are the volume, length, and width of the tumor, respectively. Rats were sacrificed when the volume exceeded 10 times the initial volume or ulceration was observed.

Assessment of skin response to treatment

The skin response to laser treatment was assessed visually and rated using the following scale: 0, no observable reaction; 1 Eschar covers less than 50% treated surface area; 2 Eschar covers more than 50% treated surface area; 3 Eschar covers >50% of treated area and is >1 mm thick.

Statistical analysis

Kaplan–Meier curves were used to analyze tumor growth inhibition efficacy with GraphPad prism (Version 5.01). Each pair of groups were compared by the Log-rank (Mantel–Cox) test. Differences were considered significant at $P < 0.05$. Median survival was defined as the time at which the staircase survival curve crosses the 50% survival point.

Use of animals and human blood samples

Human blood used for *in vitro* studies was collected in accordance with Protocol OH99-C-N046. All animal studies in this work were approved by either the University at Buffalo Institutional Animal Care and Use Committee, or by the NCI at Fredrick Institutional Animal Care and Use Committee.

Results

Liposome characterization

LC-Dox-PoP liposomes, were formed with the same composition ([DSPC:DSPE-PEG2000:Pyro-lipid:Chol] in a mol. ratio of [53:5:2:40]) as previously described (38). To conduct immunological characterization, liposomes were prepared using a protocol to minimize endotoxins to prevent contaminant interference of the results. This batch of liposomes was characterized

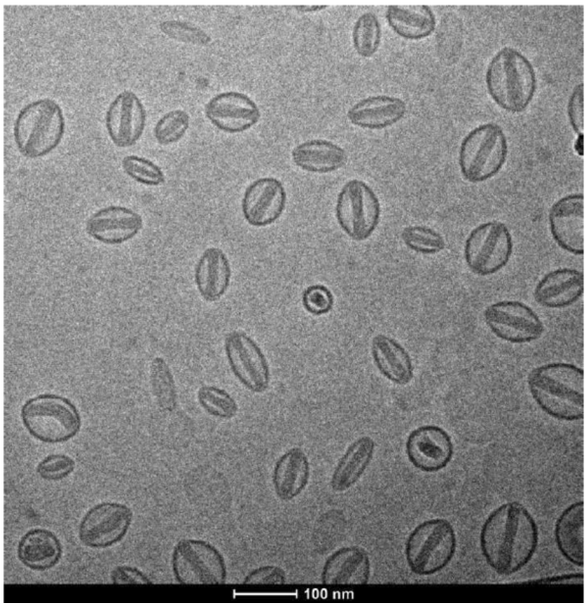

Figure 1.
Cryo-electron micrograph of LC-Dox-PoP liposomes.

for its endotoxin content (Supplementary Table S1 in the Supplementary Information), size, zeta potential, and morphology. The liposome diameter ranged from 90 to 100 nm, depending on the measurement conditions and the zeta potential showed a mild negative charge (Supplementary Table S2 in the Supplementary Information). Cryo-TEM images showed the liposomes had a somewhat elongated shape due to the presence of the prominent doxorubicin bundles contained entirely within the liposome (Fig. 1). The overall morphology is similar to the observed structure of the FDA approved liposomal doxorubicin, Doxil (14). Dox entrapment efficiency for this batch of liposomes was found to be approximately 93% as assessed using a UV-Vis microcentrifugal assay, consistent with the reported loading efficacy of >90% for Doxil (14).

Immunological characterization

The general compatibility of LC-Dox-PoP liposomes with human blood was tested *in vitro*, using an *in vivo* relevant concentration range if the liposomes were administered intravenously at a human dose level of 0.8 mg/kg, which is analogous to a 10 mg/kg mouse dose used in previous efficacy studies (39). The analysis included analysis of the effects of LC-Dox-PoP liposomes on erythrocytes, platelets, plasma coagulation cascade and the complement system.

LC-Dox-PoP liposomes were evaluated for potential particle effects on the integrity of red blood cells (Fig. 2A). Three independent samples were prepared for each test concentration and analyzed in duplicate (%coefficient of variation, CV < 20). Triton X-100 was used as a positive control (PC) and PBS as the negative control (NC). The LC-Dox-PoP liposomes were found to interfere with the hemolysis assay at all tested concentrations and the data therefore had to be normalized to account for this interference. At 0.1 mg/mL, LC-Dox-PoP liposomes appeared slightly hemolytic (hemolysis between 2% and 5%); however, at 0.2 mg/mL less hemolysis was observed.

Potential effects of LC-Dox-PoP liposomes on the cellular component of the blood coagulation cascade was evaluated at Dox concentrations ranging from 0.0004 to 0.1 mg/mL (Fig. 2B) with collagen used as the positive control. Light transmission was used to determine the presence of platelet aggregation. An increase in light transmission indicated by an increase in area under the curve (AUC) was used to indicate platelet aggregation. LC-Dox-PoP was also tested for the ability to interfere with platelet aggregation induced by collagen alone. LC-Dox-PoP liposomes added to plasma before addition of assay's positive control did not induce platelet aggregation and did not alter collagen-induced platelet aggregation at the tested concentrations (Fig. 2C).

The effects of LC-Dox-PoP liposomes on the biochemical component of the blood coagulation cascade prothrombin time, thrombin time and activated partial thromboplastin time were tested at different concentrations (Fig. 2D). Three independent samples were prepared and analyzed in duplicate (%CV <5). Normal plasma standard (Control N) and abnormal plasma standard (Control P) were used for instrument controls. LC-Dox-PoP did not alter plasma coagulation times *in vitro* for the prothrombin or activated partial thromboplastin time assays. A statistically significant prolongation of thrombin time was noted at the highest test concentration. This suggests that LC-Dox-PoP may affect either fibrinogen or thrombin or both of these proteins.

Complement activation of LC-Dox-PoP was tested at Dox concentrations ranging 0.002 to 0.66 mg/mL. PBS was used as a negative control and cobra venom factor (CVF) as a positive control. Doxil was used as an additional, clinically relevant nanoparticle for comparison. For unknown reasons, LC-Dox-PoP at all tested concentrations appeared to interfere with measurement of iC3b (detected using an inhibition/enhancement control), resulting in a diminished apparent iC3b concentration by approximately 50% (Supplementary Table S3 in the Supplementary Information). Despite this observed degree of inhibition in its detection, the amount of iC3b induced by LC-Dox-PoP in plasma were elevated, and comparable, to that observed in the Doxil-treated samples at equivalent Dox concentrations (Fig. 2E). Therefore, similar to clinical and preclinical observations with Doxil (42–45), LC-Dox-PoP could be expected to induce complement activation-related pseudoallergy (CARPA) in sensitive individuals (46, 47).

Blood partitioning

LC-Dox-PoP liposomes contain two active components, PoP (bilayer loaded) and Dox (actively loaded in the aqueous core), entrapped in different locations of the liposomes. Therefore, blood partitioning of each active drug component was measured to determine the release from LC-Dox-PoP liposomes and the partitioning of each in blood and plasma. LC-Dox-PoP was incubated in blood at three concentrations, and PoP (Fig. 2F) and Dox (Fig. 2G) plasma concentration measured at specified time points. A correlation plot (Fig. 2H) was used to compare the mean PoP and Dox percent fraction in plasma (%Fp). The data for Dox and PoP are highly correlated, falling within 30% of either side of the perfect correlation 45-degree line. Most notably, in the 0.5 μg/mL PoP concentration samples, both drugs were found in both blood and plasma equally, with a %Fp of approximately 50%, whereas in the higher 2 and 10 μg/mL PoP concentration samples, both drugs were primarily found in the plasma, with a

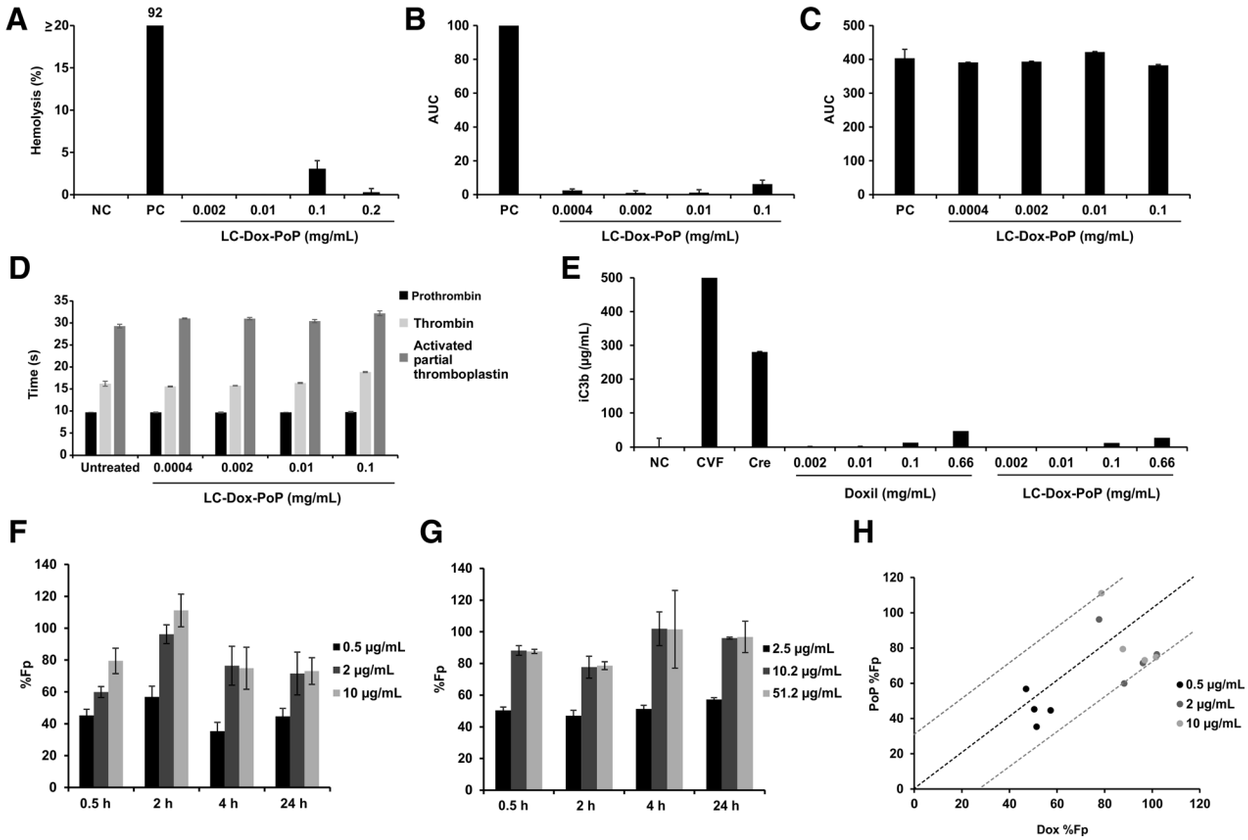

Figure 2.

In vitro effects and partitioning of LC-Dox-PoP liposomes in blood. **A,** *In vitro* hemolysis. LC-Dox-PoP appeared slightly hemolytic (hemolysis between 2% and 5%) *in vitro* at 0.1 mg/mL but not at 0.2 mg/mL. The positive control (PC) had a value of 92 but is truncated here for clarity of the lower values. PBS was used as the negative control (NC). Samples at 0.002 and 0.01 mg/mL were below lower limit of quantification (BLOQ). *In vitro* platelet aggregation was tested with Dox-PoP for (**B**) the ability to induce platelet aggregation (The positive control bar had a value of 403 but is truncated here for clarity of the lower values), and (**C**) the ability to interfere with collagen-induced platelet aggregation. Dox-PoP did not induce platelet aggregation and did not alter collagen-induced platelet aggregation at the tested concentrations. **D,** LC-Dox-PoP had no effect on prothrombin time, a statically significant (*, $P < 0.05$) increase at 0.1 mg/mL on thrombin time, and no effect on activated partial thromboplastin time. **E,** *In vitro* complement activation by LC-Dox-PoP liposomes and Doxil were tested at Dox concentrations ranging 0.002 to 0.66 mg/mL. Positive controls were cobra venom factor (CVF) and Cremophor-EL (Cre), and negative control PBS, respectively. Raw data were used to prepare the plot. The positive control bar had a value of 1,041 but is truncated here for clarity of the lower values. Samples at 0.002 and 0.01 mg/mL were below limit of quantification (BLOQ). All data shown are mean for all tests ± SD. *In vitro* blood partitioning of LC-Dox-PoP is shown as the calculated percentage of fraction in plasma (%Fp) for (**F**) PoP and (**G**) Dox as a function of time at three indicated PoP or Dox concentrations. **H,** A correlation plot of the mean PoP and Dox percentage of fraction in plasma, %Fp, data. Perfect correlation is depicted by the dashed black line running though the origin at 45 degrees. The gray dashed lines are offset from the black line by 30%. At 0.5 μg/mL LC-Dox-PoP concentration samples, both drugs are found in blood and plasma equally, with a %Fp of about 50%, whereas at 2 and 10 μg/mL PoP concentration samples, both drugs are primarily found in the plasma, with a %Fp of about 100%. Mean ± SD, $n = 3$.

%Fp of approximately 100%. This may be due to uptake of liposomes into the mononuclear blood cell fraction at lower liposome concentrations, which then saturates at higher concentrations resulting in liposome remaining in the plasma fraction. These data suggest that the LC-Dox-PoP liposomes remains intact, with both the PoP and Dox remaining associated with the liposome at the same ratios as the initial formulation.

Pharmacokinetic studies

Pharmacokinetic studies were conducted in Fischer 344 rats. Rats were intravenously administered LC-Dox-PoP liposomes at 5 mg/kg Dox. Both the PoP and Dox pharmacokinetic profiles displayed similar monophasic decays (Fig. 3A), suggesting the absence of a rapid tissue distribution phase. When normalized to injected dose, with concentrations expressed as %ID*kg/mL, the PoP and Dox profiles were superimposable (Fig. 3B), suggesting that LC-Dox-PoP liposomes are stable *in vivo* and retain both the bilayer loaded PoP and aqueous-core loaded Dox drugs in the same ratio as initially formulated. The pharmacokinetic parameters, determined by non-compartmental analysis (Supplementary Table S4 in the Supplementary Information) show as expected, the dose normalized parameters, C_L, V_{ss}, $t_{1/2}$, and MRT were very similar for both PoP and Dox, at 1.33 ± 0.10 and 1.16 ± 0.10 mL/h/kg, 45 ± 5 and 41 ± 4 mL/kg, 25 ± 1 and 26 ± 1 hour, 32 ± 2 and 33 ± 2 hour, respectively. These values are similar to those previously reported for Doxil in rats (48), indicating LC-Dox-PoP is a long circulating formulation and further evidence of stability.

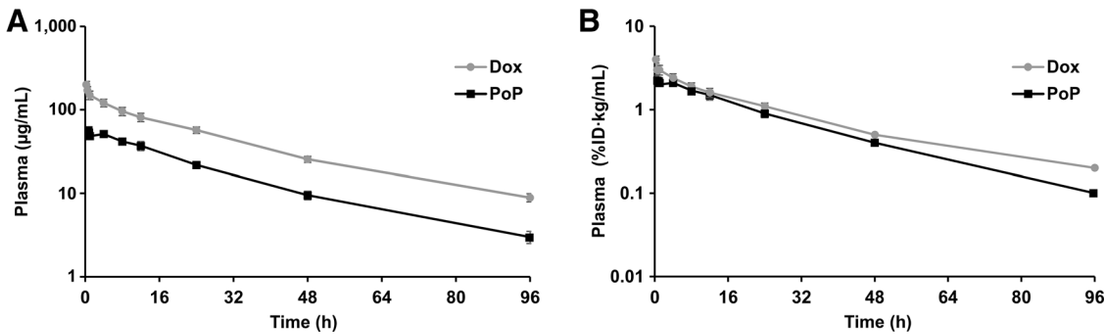

Figure 3.

Comparison of PoP and Dox pharmacokinetic profiles. 5 mg/kg LC-Dox-PoP was intravenously administered to rats. Displayed are the average PoP and Dox concentrations at each time point, expressed both as (**A**) μg/mL and (**B**) %ID*kg/mL. Mean ± S.D., $n = 6$. The PoP and Dox circulation half-lifes were 25 and 26 hours, respectively.

Biodistribution and tumor drug deposition

Tissue distribution studies were conducted in female Fischer 344 rats bearing orthotopic R3230 mammary adenocarcinoma tumors. The rats were injected with 2 mg/kg LC-Dox-PoP and treated with a 665 nm laser at a fluence rate of 150 mW/cm^2 for a total fluence of 250 J/cm^2. Similar distribution of PoP (Fig. 4A) and Dox (Fig. 4B) was observed in key organs with the majority of each accumulating in the spleen and liver, indicating that both drugs remain within the liposomes during circulation and experience clearance mechanisms. An enhancement of both PoP and Dox was also observed in the skin adjacent to light treated tumors.

Tumor uptake of PoP and Dox was studied as a function of tumor depth. Laser-treated and -untreated tumors from rats injected with 2 mg/kg LC-Dox-PoP were removed and cut into 2 mm segments with distance 0 representing the side to the tumor adjacent to the skin (the location that receives the greatest amount

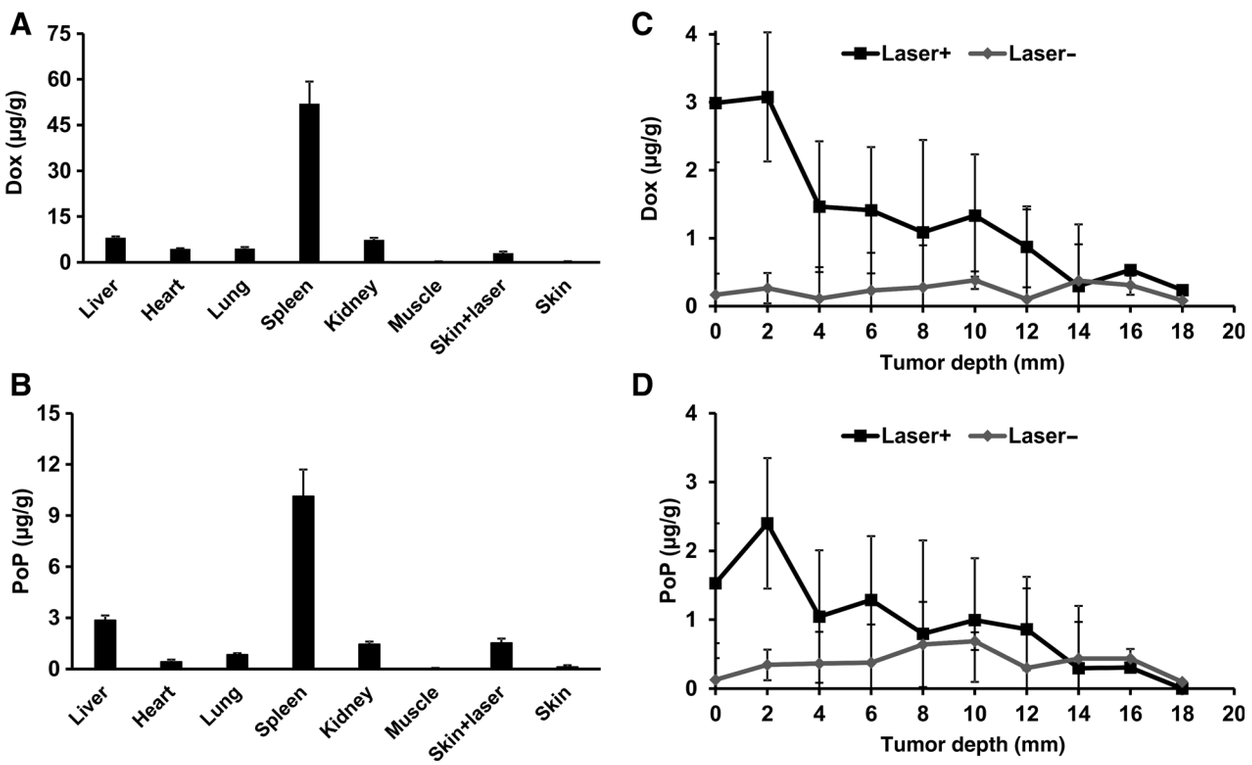

Figure 4.

Biodistribution and depth-dependent tumor drug distribution. Biodistribution of (**A**) Dox and (**B**) PoP in Fischer 344 rats inoculated with R3230 mammary adenocarcinoma orthotopic tumors 24 hours after intravenous injection with 2 mg/kg LC-Dox-PoP. Dox (**C**) and (**D**) PoP (**D**) deposition as a function of tumor depth in laser-treated (665 nm at 150 mW/cm^2 for 250 J/cm^2) and untreated orthotopic R3230 tumors. The drug–light interval was 1 hour. Data show mean ± S.D. for $n = 4$–5.

of light). Both PoP and Dox in the laser treated tumors exhibited the same trend in which drug concentration decreased as the tumor depth increased. The untreated tumors exhibited no significant change in drug concentration throughout the tumor depth. Enhancement of drug deposition was observed at tumor tissue depths to 12 mm for Dox and 10 mm for PoP, with statistically significant differences ($P < 0.05$, student T test) compared with non-irradiated tumors observed up to 6 mm for Dox (Fig. 4C) and 4 mm for PoP (Fig. 4D). Within laser-treated tumors, when compared with the amount of Dox found at 18-mm depth, significantly more Dox was found at all depths up to 12 mm ($P < 0.05$, student T test). The greater deposition range of Dox over PoP may be due to diffusion of released Dox from the liposomes. The general trend was consistent with calculated light propagation in tumor tissue, which exhibits exponential decay over tumor depth using parameters for light attenuation in breast (Supplementary Fig. S1 in the Supplementary Information; ref. 49).

Tumor growth inhibition

Female Fischer 344 rats inoculated with R3230 mammary adenocarcinoma cells orthotopically in the mammary fat pad were used in all tumor studies. In initial studies rats were injected with 2 mg/kg LC-Dox-PoP and treated with a 665 nm laser at a fluence rate of 150 mW/cm^2 for a total light dose of 250 J/cm^2 (Fig. 5A). A second group received only LC-Dox-PoP without laser (Fig. 5B) and a third an equivalent dose of empty-PoP liposomes with laser treatment (Fig. 5C). The empty-PoP liposomes (median survival 31 days) and LC-Dox-PoP liposomes without laser treatment (median survival 30 days) groups showed no significant improvement over the untreated control (median survival 26 days; Fig. 5D), whereas the laser-treated LC-Dox-PoP (median survival >90 days) showed significant improvement in tumor suppression ($P < 0.05$) over all three groups. Tumors were effectively cured in three of six rats over 90 days, whereas one tumor grew slowly over the same time. Two tumors grew at a faster rate, though slower than the tumors in the other groups. Post treatment analysis found that both of these tumors had an initial starting diameter greater than 11.5 mm.

To test whether or not the tumor size was an important factor in the therapeutic outcome of LC-Dox-PoP liposome treatment two additional groups were tested. Ten rats were split into two groups, one with tumor diameters <11.5 mm, and a second with tumor diameters >11.5 mm. Both groups were injected with 2 mg/kg LC-Dox-PoP and treated with a 665 nm laser at a fluence rate of 150 mW/cm^2 for a total light dose of 250 J/cm^2. In this study, no significant differences were found between the >11.5 mm and <11.5 mm groups with 2 of 5, and 3 of 5 rats displaying complete tumor suppression, respectively (Supplementary Fig. S2 in the Supplementary Information). However, when analyzed with the previous data, a statistically significant difference ($P < 0.05$) was observed between the two groups with median survival of 40 days and >90 days in the >11.5 mm and <11.5 mm groups, respectively (Fig. 5E). In the combined data, with treated tumors <11.5 mm, 7/9 rats survived until 90 days with 6/9 rats having cures. In comparison, for treated tumors >11.5 mm, only 2/7 survived until 90 days, with a single cure. The difference in efficacy based on tumor size may be due to light propagation limitations in the larger tumors.

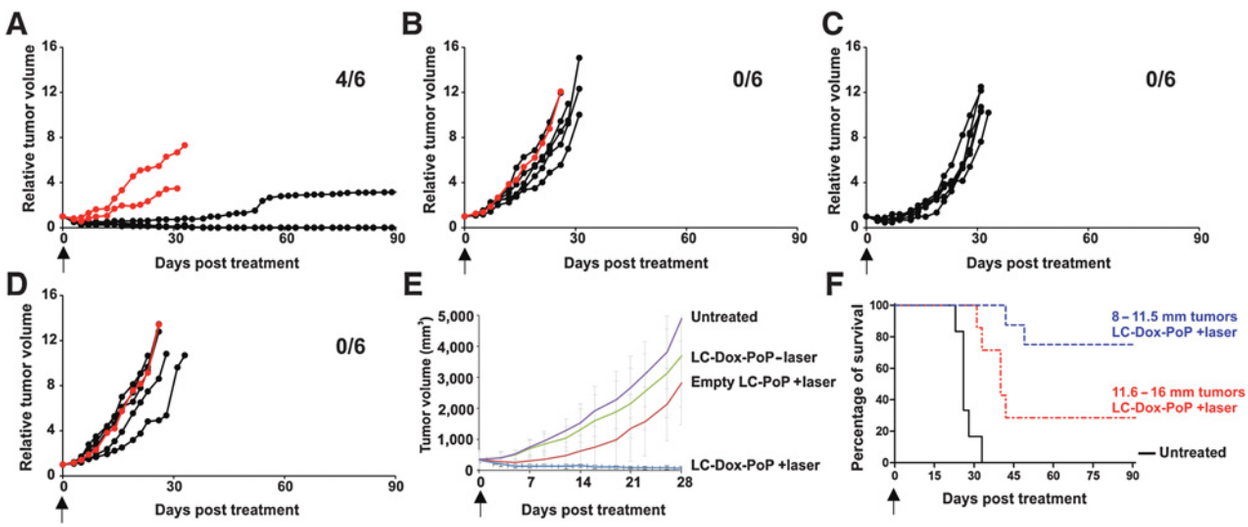

Figure 5.

Tumor growth inhibition. Fischer 344 rats bearing large orthotopic R3230 mammary adenocarcinoma tumors received a single treatment on day zero (indicated by arrows). Rats had suppressed tumor growth ($P < 0.05$) when treated with a 665-nm laser at a fluence rate of 150 mW/cm^2, 1 hour after intravenous injection with (**A**) 2 mg/kg LC-Dox-PoP liposomes with a 250 J/cm^2 laser dose; compared with (**B**) 2 mg/kg LC-Dox-PoP without laser treatment; **C,** empty-PoP liposomes with equivalent laser treatment; and (**D**) no treatment. Red lines indicate tumors larger than 11.5 mm at time of treatment. The number of surviving rats at the end of 90 days is indicated. **E,** Tumor growth curves for the untreated control; LC-Dox-PoP—laser; Empty LC-PoP + laser and LC-Dox-PoP + laser with initial tumor size <11.5 mm. A statistically significant difference (ANOVA) was observed between the LC-PoP +laser group and all other groups ($P < 0.05$) but not between any of the other groups. **F,** Kaplan–Meier survival curve. Tumor growth data from a second study were included, and rats ($n = 7$–9) were grouped based on tumor diameter at the time of laser treatment. All rats were injected with 2 mg/kg LC-Dox-PoP liposomes and received laser treatment with a 665-nm laser at a fluence rate of 150 mW/cm^2 and total light dose of 250 J/cm^2. Both groups were significantly better than the untreated control (log-rank test, $P < 0.05$), and a statistically significant difference was observed between the two groups (log-rank test, $P < 0.05$).

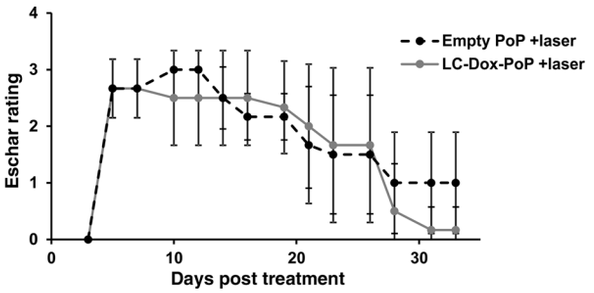

Figure 6.
Eschar healing. Fischer 344 rats inoculated with R3230 mammary adenocarcinoma orthotopic tumors were intravenously injected with 2 mg/kg LC-Dox-PoP liposomes or an equivalent dose of empty PoP liposomes and received laser treatment with a 665-nm laser at a fluence rate of 150 mW/cm^2 and total light dose of 250 J/cm^2. Eschar formation was monitored after laser treatment and rated on a 1 to 3 scale. Data show mean ± S.D.; ($n = 6$).

The light received by deeper parts of the tumor may not be therapeutically sufficient. These results are similar to clinical observation with photodynamic therapy where the greatest efficacy is observed in tumors with diameters <1 cm (50–52).

The effects of laser treatment on skin of LC-Dox-PoP and empty-PoP laser–treated rats were monitored visually immediately following laser treatment for 30 days. Eschar formation was rated on a 1 to 3 scale (See Supplementary Fig. S3 in the Supplementary Information for a description). Immediately following laser treatment mild swelling at the treatment site was observed. The following day eschar formation could be observed visually in all animals. The eschars were most intense in the first week following treatment, gradually and completely healing over the following weeks (Fig. 6).

Discussion

The purpose of these studies was to estimate general compatibility of LC-Dox-PoP with human blood at concentrations relevant to those which may occur *in vivo* when this material is intravenously administered at a human-relevant dose level (0.8 mg/kg), determine the pharmacokinetic profile of LC-Dox-PoP with emphasis on the stability of the liposome entrapped components, and test antitumor efficacy at human relevant doses at varying depths.

The effects on erythrocytes, platelets, plasma coagulation cascade, and the complement system were unremarkable in all assays with a few exceptions. The most notable of which is the activation of complement *in vitro* similar to that observed with the PEGylated liposomal doxorubicin formulation, Doxil, which is known to cause CARPA in sensitive individuals. *In vitro* blood partitioning and *in vivo* pharmacokinetics showed the liposomes to be stable retaining both the PoP and Dox at similar levels.

Laser treatment enhanced drug delivery to 1.2-cm depth in tumor tissue, and tumors with initial diameters of less than 1.2 cm had better treatment outcomes. As light diffusion through tissues is subject to rapid attenuation due to scattering and absorption, the depth of photoablation is an important parameter for planning the treatment of larger tumors using approach such as the use of multiple and interstitial optical fibers for light delivery.

A single human relevant dose of 2 mg/kg was able to potently suppress tumor growth, with antitumor synergy observed between chemo- and photocomponents. CPT using LC-Dox-PoP liposomes had a markedly improved effect compared with PDT using the same liposomes (containing the PoP photosensitizer) that lacked Dox, and to LC-Dox-PoP without the laser treatment. Despite this potent ablation efficacy, skin healing with CPT was similar to PDT.

In summary, LC-Dox-PoP liposomes appear to have similar blood behavior and immunological properties to Doxil, are stable and long circulating, and exhibit potent antitumor efficacy in a single treatment at a human relevant drug dose, lower than typically used in rats. Together, these data show that additional studies of LC-Dox-PoP are warranted, including assessing additional treatment efficacy in different tumor types, assessing impact of varying drug and light doses, and testing CPT in larger animals.

Disclosure of Potential Conflicts of Interest

K.A. Carter is a scientist and has ownership interest (including stock, patents, etc.) in POP Biotechnologies. J.F. Lovell has ownership interest (including stock, patents, etc.) in POP Biotechnologies. No potential conflicts of interest were disclosed by the other authors.

Disclaimer

The content of this publication does not necessarily reflect the views or policies of the Department of Health and Human Services, nor does mention of trade names, commercial products, or organizations imply endorsement by the U.S. government.

Authors' Contributions

Conception and design: K.A. Carter, S.T. Stern, J.F. Lovell
Development of methodology: K.A. Carter, S.T. Stern, J.F. Lovell
Acquisition of data (provided animals, acquired and managed patients, provided facilities, etc.): K.A. Carter, D. Luo, J. Geng
Analysis and interpretation of data (e.g., statistical analysis, biostatistics, computational analysis): K.A. Carter, D. Luo, S.T. Stern, J.F. Lovell
Writing, review, and/or revision of the manuscript: K.A. Carter, S.T. Stern, J.F. Lovell
Administrative, technical, or material support (i.e., reporting or organizing data, constructing databases): J. Geng, J.F. Lovell
Study supervision: J.F. Lovell

Acknowledgments

This work was supported by the National Institutes of Health (R01EB017270 and DP5OD017898; to J.F. Lovell) and the National Science Foundation (1555220; to J.F. Lovell).The formulation described herein was characterized by the Nanotechnology Characterization Laboratory as part of its free Assay Cascade characterization service for cancer nanomedicines, which is supported by the National Cancer Institute, National Institutes of Health, under Contract No. HHSN261200800001E (to S.T. Stern).

Received May 22, 2018; revised September 28, 2018; accepted December 13, 2018; published first December 26, 2018.

References

1. Minchinton AI, Tannock IF. Drug penetration in solid tumours. Nat Rev Cancer 2006;6:583.
2. Tannock IF, Lee CM, Tunggal JK, Cowan DSM, Egorin MJ. Limited penetration of anticancer drugs through tumor tissue: a potential cause of

resistance of solid tumors to chemotherapy. Clin Cancer Res 2002;8: 878–84.
3. Luo D, Carter KA, Lovell JF. Nanomedical engineering: shaping future nanomedicines. Wiley Interdiscip Rev Nanomed Nanobiotechnol 2015;7: 169–88.
4. Allen TM, Cullis PR. Drug delivery systems: entering the mainstream. Science 2004;303:1818–22.
5. Allen TM, Cullis PR. Liposomal drug delivery systems: from concept to clinical applications. Adv Drug Deliv Rev 2013;65:36–48.
6. Wei A, Mehtala JG, Patri AK. Challenges and opportunities in the advancement of nanomedicines. J Control Release 2012;164: 236–46.
7. Paliwal SR, Paliwal R, Agrawal GP, Vyas SP. Liposomal nanomedicine for breast cancer therapy. Nanomed 2011;6:1085–100.
8. Chang HI, Yeh MK. Clinical development of liposome-based drugs: formulation, characterization, and therapeutic efficacy. Int J Nanomedicine 2012;7:49–60.
9. O'Brien ME, Wigler N, Inbar M, Rosso R, Grischke E, Santoro A, et al. Reduced cardiotoxicity and comparable efficacy in a phase III trial of pegylated liposomal doxorubicin HCl (CAELYX/Doxil) versus conventional doxorubicin for first-line treatment of metastatic breast cancer. Ann Oncol 2004;15:440–9.
10. Kong G, Anyarambhatla G, Petros WP, Braun RD, Colvin OM, Needham D, et al. Efficacy of liposomes and hyperthermia in a human tumor xenograft model: importance of triggered drug release. Cancer Res 2000; 60:6950–7.
11. Kadam RS, Bourne DW, Kompella UB. Nano-advantage in enhanced drug delivery with biodegradable nanoparticles: contribution of reduced clearance. Drug Metab Dispos 2012;40:1380–8.
12. De Jong WH, Borm PJ. Drug delivery and nanoparticles: applications and hazards. Int J Nanomedicine 2008;3:133–49.
13. Singh R, Lillard JW. Nanoparticle-based targeted drug delivery. Exp Mol Pathol 2009;86:215–23.
14. Barenholz Y. Doxil®—the first FDA-approved nano-drug: lessons learned. J Controlled Release 2012;160:117–34.
15. Lao J, Madani J, Puértolas T, Álvarez M, Hernández A, Pazo-Cid R, et al. Liposomal doxorubicin in the treatment of breast cancer patients: a review. J Drug Deliv 2013;456409.
16. Rafiyath SM, Rasul M, Lee B, Wei G, Lamba G, Liu D. Comparison of safety and toxicity of liposomal doxorubicin vs. conventional anthracyclines: a meta-analysis. Exp Hematol Oncol 2012;1:10.
17. Safra T, Muggia F, Jeffers S, Tsao-Wei DD, Groshen S, Lyass O, et al. Pegylated liposomal doxorubicin (doxil): reduced clinical cardiotoxicity in patients reaching or exceeding cumulative doses of 500 mg/m2. Ann Oncol 2000;11:1029–33.
18. Gabizon AA. Pegylated liposomal doxorubicin: metamorphosis of an old drug into a new form of chemotherapy. Cancer Invest 2001;19: 424–36.
19. Gabizon A, Catane R, Uziely B, Kaufman B, Safra T, Cohen R, et al. Prolonged circulation time and enhanced accumulation in malignant exudates of doxorubicin encapsulated in polyethylene-glycol coated liposomes. Cancer Res 1994;54:987–92.
20. Rivera E, Valero V, Esteva FJ, Syrewicz L, Cristofanilli M, Rahman Z, et al. Lack of activity of stealth liposomal doxorubicin in the treatment of patients with anthracycline-resistant breast cancer. Cancer Chemother Pharmacol 2002;49:299–302.
21. Cao J, Li C, Wei X, Tu M, Zhang Y, Xu F, et al. Selective targeting and eradication of LGR5+ CSCs using RSPO conjugated doxorubicin liposomes. Mol Cancer Ther 2018; 27:1475–85.
22. Sattiraju A, Xiong X, Pandya DN, Wadas TJ, Xuan A, Sun Y, et al. Alpha particle enhanced blood brain/tumor barrier permeabilization in glioblastomas using integrin Alpha-v Beta-3–targeted liposomes. Mol Cancer Ther 2017;16:2191–200.
23. Shmeeda H, Mak L, Tzemach D, Astrahan P, Tarshish M, Gabizon A. Intracellular uptake and intracavitary targeting of folate-conjugated liposomes in a mouse lymphoma model with up-regulated folate receptors. Mol Cancer Ther 2006;5:818–24.
24. Tung HY, Su YC, Chen BM, Burnouf PA, Huang WC, Chuang KH, et al. Selective delivery of PEGylated compounds to tumor cells by anti-PEG hybrid antibodies. Mol Cancer Ther 2015;14:1317–26.
25. Needham D, Dewhirst MW. The development and testing of a new temperature-sensitive drug delivery system for the treatment of solid tumors. Adv Drug Deliv Rev 2001;53:285–305.
26. Ganta S, Devalapally H, Shahiwala A, Amiji M. A review of stimuli-responsive nanocarriers for drug and gene delivery. J Controlled Release 2008;126:187–204.
27. Preiss MR, Bothun GD. Stimuli-responsive liposome-nanoparticle assemblies. Expert Opin Drug Deliv 2011;8:1025–40.
28. Nicolas J, Couvreur P, Mura S. Stimuli-responsive nanocarriers for drug delivery. Nat Mater 2013;12:991.
29. Shum P, Kim JM, Thompson DH. Phototriggering of liposomal drug delivery systems. Adv Drug Deliv Rev 2001;53:273–84.
30. Timko BP, Dvir T, Kohane DS. Remotely triggerable drug delivery systems. Adv Mater 2010;22:4925–43.
31. Spring BQ, Sears RB, Zheng LZ, Mai Z, Watanabe R, Sherwood ME, et al. A photoactivable multi-inhibitor nanoliposome for tumour control and simultaneous inhibition of treatment escape pathways. Nat Nanotechnol 2016;11:378–87.
32. Zagar TM, Vujaskovic Z, Formenti S, Rugo H, Muggia F, O'Connor B, et al. Two phase I dose-escalation/pharmacokinetics studies of low temperature liposomal doxorubicin (LTLD) and mild local hyperthermia in heavily pretreated patients with local regionally recurrent breast cancer. Int J Hyperthermia 2014;30:285–94.
33. Poon RT, Borys N. Lyso-thermosensitive liposomal doxorubicin: a novel approach to enhance efficacy of thermal ablation of liver cancer. Expert Opin Pharmacother 2009;10:333–43.
34. Tak WY, Lin SM, Wang Y, Zheng J, Vecchione A, Park SY, et al. Phase III HEAT study adding lyso-thermosensitive liposomal doxorubicin to radiofrequency ablation in patients with unresectable hepatocellular carcinoma lesions. Clin Cancer Res 2018;24:73–83.
35. Luo D, Carter KA, Miranda D, Lovell JF. Chemophototherapy: an emerging treatment option for solid tumors. Adv Sci 2017;4: 1600106.
36. Agostinis P, Berg K, Cengel KA, Foster TH, Girotti AW, Gollnick SO, et al. Photodynamic therapy of cancer: an update. CA Cancer J Clin 2011;61: 250–81.
37. Celli JP, Spring BQ, Rizvi I, Evans CL, Samkoe KS, Verma S, et al. Imaging and photodynamic therapy: mechanisms, monitoring, and optimization. Chem Rev 2010;110:2795–838.
38. Luo D, Carter KA, Razi A, Geng J, Shao S, Giraldo D, et al. Doxorubicin encapsulated in stealth liposomes conferred with light-triggered drug release. Biomaterials 2016;75:193–202.
39. Ahsan B, Pfeifer BA, Scholes CP, Luo D, Zhang G, Huang H, et al. Porphyrin–phospholipid liposomes permeabilized by near-infrared light. Nat Commun 2014;5:3546.
40. Luo D, Carter KA, Razi A, Geng J, Shao S, Lin C, et al. Porphyrin-phospholipid liposomes with tunable leakiness. J Control Release 2015; 220:484–94.
41. Zolnik BS, Stern ST, Kaiser JM, Heakal Y, Clogston JD, Kester M, et al. Rapid distribution of liposomal short-chain ceramide in vitro and in vivo. Drug Metab Dispos Biol Fate Chem 2008;36:1709–15.
42. Wibroe PP, Ahmadvand D, Oghabian MA, Yaghmur A, Moghimi SM. An integrated assessment of morphology, size, and complement activation of the PEGylated liposomal doxorubicin products Doxil®, Caelyx®, DOXOrubicin, and SinaDoxosome. J Controlled Release 2016;221:1–8.
43. Moghimi SM, Szebeni J. Stealth liposomes and long circulating nanoparticles: critical issues in pharmacokinetics, opsonization and protein-binding properties. Prog Lipid Res 2003;42:463–78.
44. Szebeni J, Baranyi L, Savay S, Lutz HU, Jelezarova E, Bunger R, et al. The role of complement activation in hypersensitivity to pegylated liposomal doxorubicin (Doxil®). J Liposome Res 2000; 10:467–81.
45. Chanan-Khan A, Szebeni J, Savay S, Liebes L, Rafique NM, Alving CR, et al. Complement activation following first exposure to pegylated liposomal doxorubicin (Doxil): possible role in hypersensitivity reactions. Ann Oncol 2003;14:1430–7.
46. Szebeni J. Complement activation-related pseudoallergy: a new class of drug-induced acute immune toxicity. Toxicology 2005;216: 106–21.

47. Szebeni J. Complement activation-related pseudoallergy caused by liposomes, micellar carriers of intravenous drugs, and radiocontrast agents. Crit Rev Ther Drug Carr Syst [Internet]. 2001 [cited 2017 Nov 26. Available from: http://www.dl.begellhouse.com/journals/3667c4ae6e8fd136, 2dbee23b005233cf,7665cee60b7f8e89.html.
48. Gabizon A, Shmeeda H, Barenholz Y. Pharmacokinetics of pegylated liposomal doxorubicin. Clin Pharmacokinet 2003;42:419–36.
49. Jacques SL. Optical properties of biological tissues: a review. Phys Med Biol 2013;58:R37.
50. Simone CB, Friedberg JS, Glatstein E, Stevenson JP, Sterman DH, Hahn SM, et al. Photodynamic therapy for the treatment of non-small cell lung cancer. J Thorac Dis 2012;4:63–75.
51. Quirk BJ, Brandal G, Donlon S, Vera JC, Mang TS, Foy AB, et al. Photodynamic therapy (PDT) for malignant brain tumors – where do we stand? Photodiagnosis Photodyn Ther 2015;12:530–44.
52. Huang Z, Xu H, Meyers AD, Musani AI, Wang L, Tagg R, et al. Photodynamic therapy for treatment of solid tumors – potential and technical challenges. Technol Cancer Res Treat 2008;7:309–20.